Nonlinear Axial Combustion Instability in Solid Propellant Motors

W G BROWNLEE*
Canadian Armament Research and Development Establishment, Valcartier, Quebec, Canada

Nonlinear axial combustion instability occurs when one or more strong gaseous compression waves propagate longitudinally within a solid propellant rocket motor The nonlinear unsteady flow field derives energy through interaction with the combustion process and causes an increase in the time-averaged burning rate, pressure, and thrust This behavior has been investigated using polyurethane-ammonium perchlorate propellants and some 200 motors in the size range 2-in -diam × 10-in -long to 17-in -diam × 180-in -long Reproducible results were obtained The motors were found to be linearly stable and nonlinearly unstable with respect to initiation of instability Thus, normal proof firings are unlikely to detect inherent instability, since a flow disturbance of finite amplitude is required to trigger the system A pulse injection method of triggering was applied to all firings As operating pressures increased above a critical value P_s^* the motors became capable of instability, the severity increasing monotonically with the restriction ratio The effect on P^* of changing the motor scale, length to diameter ratio, grain cross section, grain temperature, and of adding aluminum alloy and lithium fluoride to the propellant was determined

Nomenclature

A_t = area of nozzle throat
c^* = characteristic exhaust velocity of propellant
C_p^0 = heat capacity at constant pressure at 1 atm and temperature noted in text, cal deg^{-1}-mole^{-1}
D_p = diameter of propellant grain port or perforation
d_t = diameter of nozzle throat
f_w = fraction of web thickness consumed
J = ratio of nozzle throat area to port area
k = parameter in empirical relation $\bar{P}_u = kK_n^\beta$
K_n = ratio of burning surface area to nozzle throat area
K_{ni} = value of K_n at $t = 0$
K_n^* = value of K_n which defines beginning of unstable regime
L_p = length of propellant grain
n = ballistic parameter in burning rate law $r = \alpha P^n$
$\bar{P}$ = chamber pressure (stable or unstable) as recorded by low-frequency-response system
P = stable chamber pressure (no erosion)
P^* = stable chamber pressure (erosive conditions)
$\bar{P}_u^*$ = stable pressure when $K_n = K_n^*$ (erosive conditions)
$\bar{P}_u$ = time averaged value of unsteady chamber pressure as recorded by low frequency-response system
r = linear burning rate of propellant during stable nonerosive operation
t = time from ignition
$t_{a\,3p}$ = 30 psi action time
T_p = prefiring temperature of propellant
α = ballistic parameter in burning rate law $r = \alpha P^n$
β = parameter in empirical relation $\bar{P}_u = kK_n^\beta$
γ = ratio of specific heats
ρ_p = density of propellant

$$\phi = \int_0^t A_t \bar{P} dt \Big/ \int_0^{t_{a\,3p}} A_t \bar{P} dt$$

Introduction

NONLINEAR axial combustion instability occurs when one or more strong compression waves propagate longitudinally within the cavity of a solid propellant rocket motor The resulting unsteady flow field interacts with the combustion process, derives energy from the interaction, and causes an increase in the time-space-averaged burning rate of the propellant Consequently, the average levels of the chamber pressure and thrust rise above their normal values At the same time, high-intensity fluctuations in the instantaneous pressure and thrust levels occur at the frequency of oscillation Since the over-pressure margin for flight motors is small, instability of moderate intensity will usually cause structural failure; this process may be accelerated by the increased heat-transfer rates associated with unsteady flow conditions If, on the other hand, the motor retains its mechanical integrity, the flight vehicle continues to be subjected to mechanical vibrations and accelerations that are excited by the oscillating thrust level It is evident, therefore, that stable operation should be a proved characteristic of a design motor

The most straightforward demonstration of stability usually has been considered to be normal proof firings In the present instance, however, it was found that such firings provided no guarantee whatsoever Experimental results show that finite-wave axial instability is linearly stable and nonlinearly unstable with respect to initiation A threshold effect exists such that motors capable of catastrophic instability will repeatedly operate in a stable manner provided that any natural flow disturbances that occur are of sufficiently small amplitude On the other hand, any relatively large disturbance may suffice to trigger the instability

The present investigation, which began in 1960, was aimed at determining the detailed characteristics of nonlinear axial instability Initial efforts were directed toward development of a multiple-pulse technique for the injection of trigger flow disturbances Reproducible unstable motor behavior was then obtained, provided that the stable ballistic characteristics of the propellants were well controlled In subsequent experiments, the approach taken was to observe the behavior of unstable motors as various operating parameters were varied from firing to firing Information was sought on the effect of changing the operating pressure level, the grain cross section, the motor diameter and length, and the associated area-ratios, as well as the scale From these firings, a correlation of motor behavior was obtained which led to an approximate criterion for stable operation Further experiments were made in which various aluminum powders were substituted for a portion of the propellant oxidizer, and in one instance the burning rate-depressant

Presented as Preprint 63-228 at the AIAA Summer Meeting, Los Angeles, Calif, June 17–20, 1963; revision received November 20, 1963 This investigation was conducted as a Propulsion Wing program with the support of other CARDE facilities The author wishes to thank all those who participated for their cooperation, untiring efforts, and their ingenious solutions of the many problems encountered

* Major, Royal Canadian Artillery; seconded to Defence Research Board, Canada; Ballistic Group Leader, Rocket Engine Development Section Member AIAA

lithium fluoride was added In all, some 200 motors were fired in the size range 2-in -case-i.d × 10-in -long to 17-in - case-i d × 180-in -long, using the polyurethane-ammonium perchlorate propellants described in Table 1

The formulation changes were hardly comprehensive, since they were dictated by the necessity of making early use of the results in development work [1] Furthermore, the behavior of propellant systems based on other binders was not evaluated Nevertheless, the firing results provide a preliminary description of motor behavior as a function of geometry and of the ballistic characteristics and prefiring temperature of the propellants tested Finally, it is known that axial instability is not limited to the polyurethane system, since the phenomenon was observed in a firing of a 5-in - case i d × 50-in -long motor using plastic propellant [2]

History of a Typical Axially Unstable Motor

It appears advantageous to discuss a typical firing in some detail in order to describe certain general features of motor behavior and to introduce nomenclature Figure 1 shows pressure-time curves for a cylindrically perforated (4-in - port-i d) grain of propellant A_3 in an 8-in -i d × 80-in -long heavy-walled casing (A3-× 4-× 8-× 80-in motor) † The time-averaged pressure traces at the top of the figure illustrate unstable and stable (dashed line) operation At 2 7 sec, instability was triggered by a flow disturbance that was injected through the head end of the motor The steady component of the fluctuating chamber pressure $\bar{P}_u$ increased monotonically above the corresponding stable value P_s until a safety diaphragm ruptured ‡ Detailed data reduction showed that the progressive deviation between $\bar{P}_{us}$ and P was associated with an increase in the space-time-averaged burning rate On the other hand, although the amplitude of the compression wave also increased with time, the ratio

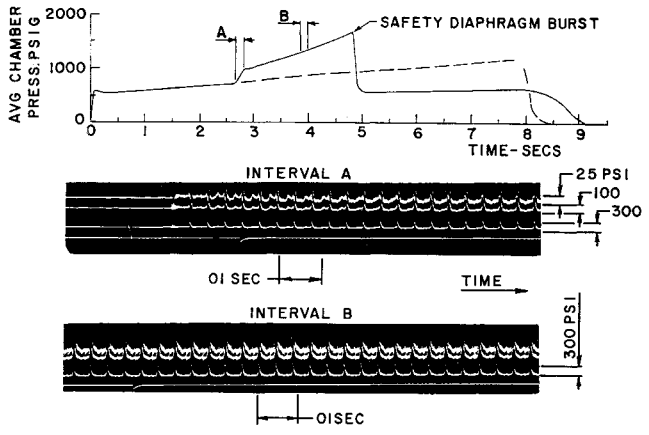

Fig 1 Pressure history of a typical unstable firing; A_3-× 4-× 8-× 80-in motor; pulse initiation

† The leading letter digit group (A_3) of this coding identifies the propellants listed in Table 1 The first number (4) is the conduit diameter in inches of a case-bonded, cylindrically perforated, end restricted grain Noncylindrical cross sections are identified by name (star, slab, etc) and are shown in Fig 2 The inside diameter of the motor casing is given by the second number (8), whereas the last number (80) is the parallel length of the casing in inches (and the nominal propellant grain length) All casings were heavy-walled except for the flight-type 17- × 180-in size

‡ Baldwin SR4 pressure transducers in conjunction with Honeywell 119 Carrier Amplifiers were used to measure the time-averaged pressure $\bar{P}_{cus}$ The demodulated output was recorded on a model 906 Visicorder after low-pass filtering The system response was intentionally limited to be down 3 db at approximately 100 cps The recorded output is thus an average of the unsteady pressure as sensed at the head end of the motors

Table 1 Propellant data[a]

Formulation code no 4760/	A_3	A_5	A_{12}	B_7	C_2
Polyurethane fuel, wt %	25	25	25	25	25
Ammonium perchlorate (150 μ), wt %	75	70	70	70	56
Aluminum, wt %					
SAX3 (40 μ, 6% Mg)		5		5	
SA24 (7 μ)			5		
SAX9 (40 μ, 12% Si)					19
LiF, added parts				1 8	
Flame temperature, °K (theoretical)	2288	2447	2447	2350	2667
Burning rate at 1000 psi, in /sec	0 19	0 20	0 22	0 15	0 14
Gaseous reaction products					
Mean molecular weight	22 49	21 00	21 00	21 06	17 84
C_p^0, cal-deg^{-1}-mole^{-1}	10 23	9 92	9 92	9 83	8 96
γ	1 24	1 25	1 25	1 25	1 29
Liquid reaction product Al_2O_3					
wt %	0	9 30	9 30	9 22	27 7
C_p^0, cal-deg^{-1} mole^{-1}	.	34.9	34 9	34 6	35 0

Thermodynamic properties are given at the flame temperature and at mospheric pressure

of peak to minimum pressure, which is a measure of the strength of the wave, tended to remain constant Sample pressure traces from a recording system with a high-frequency response are shown in the middle and bottom film strips of Fig 1 § The film strip labeled "interval A" shows the onset of instability The injected flow disturbance traversed the length of the motor, partially reflected at the nozzle end, and became a steep-fronted shock-type wave in one cycle The frequency of oscillation was about 250 cps

The lower film strip shows the compression wave during a later phase of instability (interval B) Each wave produced a jump in pressure from a minimum of approximately 1250 psi to a peak of 1750 psi, i e , a pressure ratio of about 1 4 Application of the one-dimensional theory for reflection of a plane shock wave (γ = 1 24) leads to a propagation Mach number of 1 08 with respect to the stagnant gas immediately adjacent to the head plate

It is clear from the film strips that a rapid expansion process took place at the head end immediately after each reflection of the compression wave Subsequently, the head-end pressure decreased only slightly in the remaining interval until recompression A step increment in the minimum pressure occurred in each cycle Approximately the same situation existed at the nozzle end of the motor Fastax photographs (4000 frames/sec) of the nozzle jet clearly show the arrival of the compression wave followed by a rapid relaxation to almost steady flow A sequence of frames from a similar firing is reproduced in Fig 3 The first two frames show the jet just before the arrival of the compression wave The increased mass flow produced by the compression wave (frame 3) caused the jet to broaden and the edge of the luminous zone to jump forward toward the nozzle exit Within the next three frames, i e , by frame 6, the jet had relaxed and remained almost undisturbed until recompression of the inlet gas in frame 22 Thus, as the pressure records suggest, the jet was essentially steady for the major portion of each cycle

§ All such recordings are from Kistler 401 piezo pressure transducers mounted flush in the head plate of the motors and aligned axially The output of each of two transducers was displayed on a Tektronix 551CA oscilloscope and photographed on 35 mm strip film with an Electronic Tube Corporation 5M100 camera The film strips of Fig 1 show three a c -coupled outputs at various sensitivities In later examples a d c -coupled trace is included

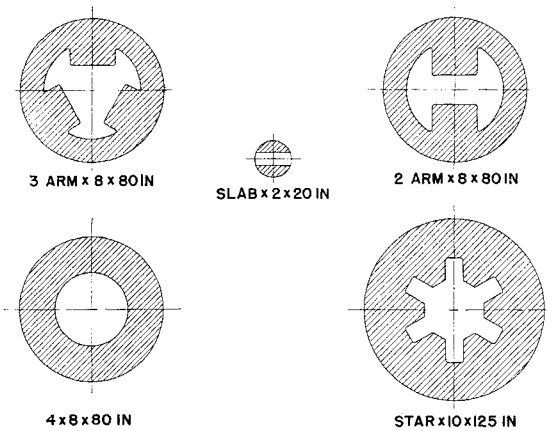

Fig 2 Grain cross sections

The frequency range of nonlinear axial instability extends from at least 110 cps to 2 kc/sec Sample pressure traces from star- × 17- × 180-in , 1- × 2- × 20-in , and 1- × 2- × 10 in motors are given in Fig 4 The corresponding frequencies are 110 cps, 1 kc/sec, and 2 kc/sec When all firings are considered, the frequencies observed to date are 110, 250, 500, and 670 cps, and 1 kc/sec and 2 kc/sec

Nonlinear Amplification and Initiation

A pulse injection system that employed so-called "sonance tubes" was devised by Dickinson[3] in 1958 These tubes, 1 5-in i d by up to 40-in long, were fitted to the head-ends of experimental 3-Arm- × 8- × 40-in motors A small gun powder charge was fired into the distant end of the tube at a preselected time during the test run In the present investigation, the mechanics of Dickinson's technique were greatly modified to reduce head-end losses and to permit multiple pulsing [4–7] The "sonance tube" was discarded in favor of screwing small pulse-charge tubes directly into the motor head plate as shown in Fig 5 The pulse tubes were charged with ICI grade FFF gun powder, sealed with a shoulder-seated steel diaphragm, epoxy resin, and W P Fuller type 3998 Seam Sealing Compound The 8-in -, 10-in , and 17-in -diam motors accommodated four such tubes, whereas three tubes were used in 2-in motor firings Powder charges were 350 mg, 11 g, and 15 g for the 2-, 8-, and 10- or 17-in motors, respectively During a given firing, the charges were electrically initiated at preselected times by an electromechanical programmer All experimental motors were tested by means of this technique In addition, the method is currently used to qualify development motors [1]

The response of motors subjected to pulse injection is nonlinear in that the system gain is a function of disturbance

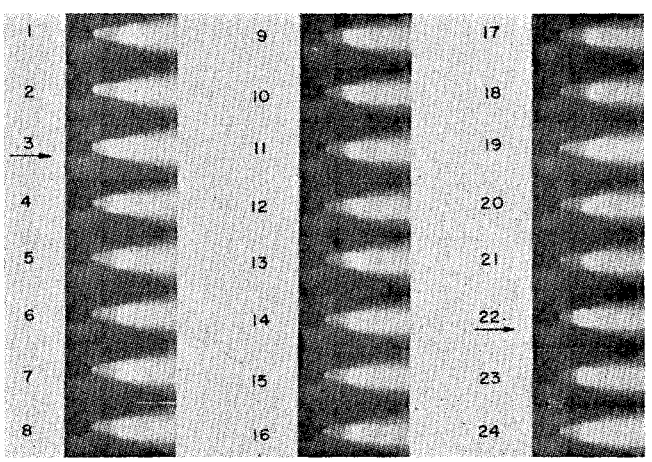

Fig 3 Fastax photographs of exhaust jet; B_7- × 3- × 8- × 80-in (4000 frames/sec)

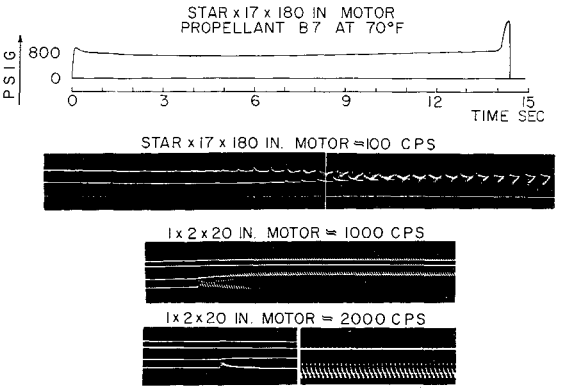

Fig 4 Typical pressure waveforms

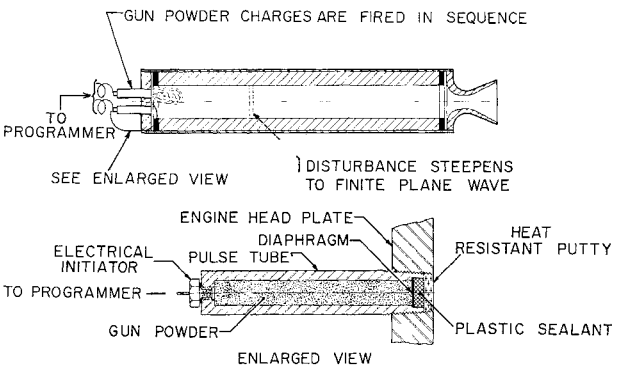

Fig 5 Pulse triggering layout

amplitude Thus, in Fig 6 an A_5- × 1- × 2-× 20-in motor appears marginally stable on the second pulse as evidenced by the decaying amplitude of the compression wave Nevertheless, during this decay period the motor became fully unstable on injection of the strong third pulse Similar nonlinear effects have been observed in many firings On the other hand, no instances of amplification from the "noise" level have been encountered It should not be inferred, however, that large-amplitude triggers are always required to induce instability

The amount of triggering necessary for initiation depends on the degree of inherent instability Although the relationship has not been investigated in detail, it appears that the more inherently unstable a motor, the smaller the required trigger The firing in Fig 1 remained stable until injection of a large triggering flow disturbance, since the only other excitation available was at the acoustic noise level On the other hand, the B_7-× star-× 17-× 180-in motor discussed in connection with Fig 4 was destroyed by self-excited axial instability At 14 sec after ignition, instability was initiated by a small flow anomaly of unknown origin On the fiftieth cycle of oscillation, the motor casing burst It will be shown later that the design of this motor placed its operating point in a region of extreme inherent instability As a further example, pressure traces from a firing of an A_8-× 1-× 2-× 30-in motor are shown in Fig 7 This motor was pulsed three times soon after ignition and remained stable Much later, when the motor was capable of severe instability, a 7-psi natural flow disturbance caused initiation when the stable pressure was 915 psia ¶

The pulse disturbances used in the testing of both developmental and experimental motors are larger than any natural anomaly likely to occur This choice gives a maximum chance for initiation and insures positive testing It has been found, however, that if the charge is excessively large a secondary effect appears The chamber pressure drops

¶ It is shown in the next section that tubularly perforated motors become more inherently unstable as the propellant is consumed

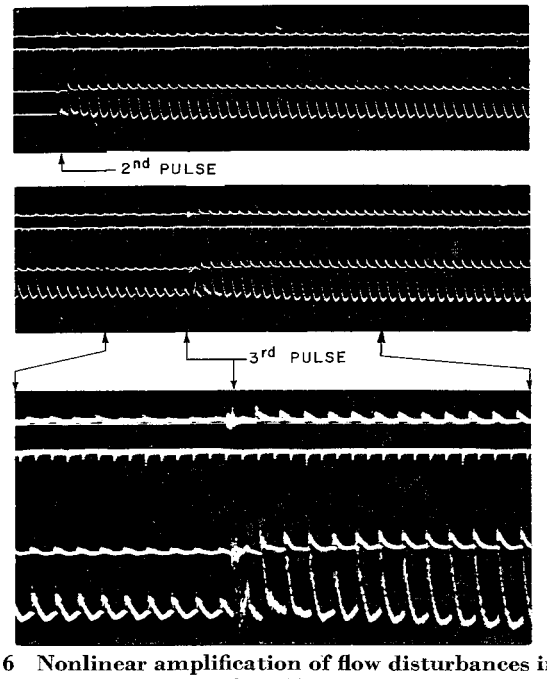

Fig 6 Nonlinear amplification of flow disturbances in an A_5-× 1-× 2-× 20-in motor

below normal while the wave decays This result is probably due to blow-off of the flame on a portion of the surface of the propellant The charge sizes noted earlier are a compromise based on a trial-and-error selection

Dependence of Axial Instability on the Restriction Ratio K_n

The effect of varying the motor geometry has been investigated with a large number of firings The most crucial result is that the degree of instability (for a given propellant and motor scale) is almost entirely dependent on the ratio of burning surface area to throat area, i e , the restriction ratio K_n A correlation was found between the steady component of the fluctuating chamber pressure $\bar{P}_u$ and K_n which permits delineation of stable and unstable operating regimes Before turning to the experiments that establish this correlation, it is first necessary to consider a peculiarity of the stable burning characteristics of the propellants listed in Table 1

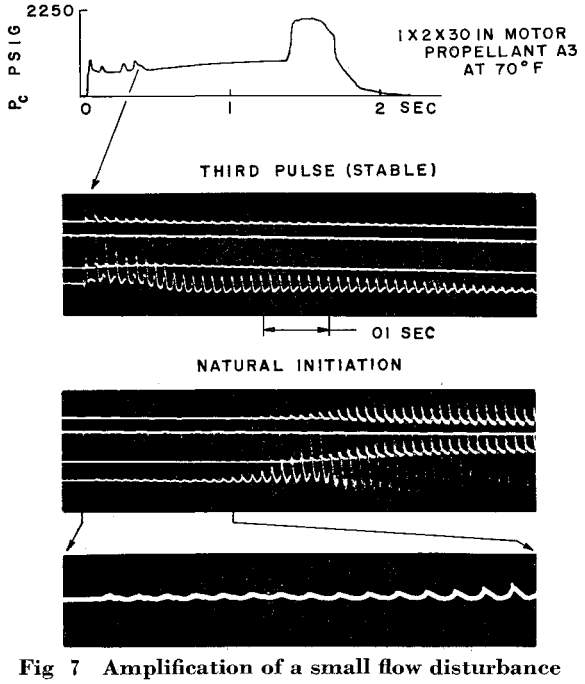

Fig 7 Amplification of a small flow disturbance

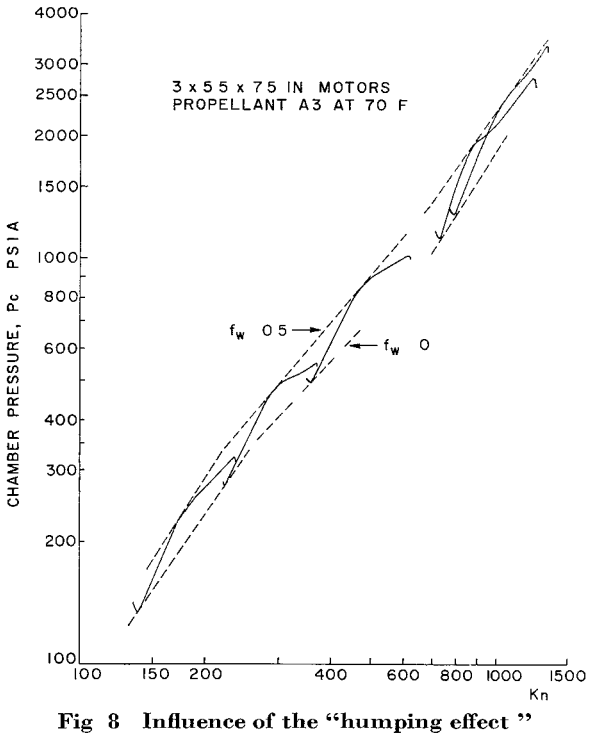

Fig 8 Influence of the "humping effect"

Stable Burning Characteristics

The propellants under investigation are subject to what is locally termed the "humping effect" The "constants" in the nonerosive rate law

$$r = \alpha P_c^n \tag{1}$$

are weak functions of the fraction of the web burnt f_w At constant pressure the rate increases until $f_w \simeq 0\,5$ and then decreases to burnout The value of r at $f_w = 1\,0$ exceeds that at $f_w = 0$ It has been established definitively that this phenomenon is associated with the structure of the propellant and in no way with flow effects, radiative heat transfer, etc [8] The tests conducted so far do not, however, define the rate-altering mechanism In any case, the effect leads to nonlinear plots in the $\log P_c - \log K_n$ plane as shown in Fig 8 It was found that the pressure values during unstable operation reflected the "humping effect" Therefore, in order to compare data for propellant with fixed properties, it was necessary to examine firing results at particular values of the web fraction ** Series of firings, interpreted in this manner, gave reproducible results; therefore, this procedure was employed whenever sufficient firing data were available

Pressure Correlations with the Restriction Ratio K_n

Pressure-time curves obtained from a series of A_5-× 1-× 2-× 20-in motors are shown in Fig 9 The traces are arranged in ascending order of the initial value of the restriction ratio K_{ni} Motors with successively smaller throat sizes became progressively more unstable and at earlier times until at $K_{ni} = 392$ instability began on ignition This be-

** K_n, f_w, etc , were calculated from average pressure data by digital computer reduction The computer program assumed uniform radial burning and thus neglected erosion effects The initial values are correct by definition, whereas later values correspond to the cylindrical volume equivalent of the erosion-tapered conduit The errors introduced by this approximation are small and about the same for each firing in a series

havioral pattern was observed in all unstable firings regardless of propellant type, grain cross section, grain temperature, and motor size or scale

Pressure data from a similar series of A_3-× 1-× 2-× 20-in motors are plotted logarithmically vs logK_n in Fig 10 All values are head-end pressures taken when the web fraction was 0 8 The curves labeled "peak" and "minimum" refer to the maximum pressure at reflection of the compression wave and the minimum pressure just prior to reflection The recorded average value of the waveforms is given by the curve labelled "average ($\bar{P}_{cu}$)"

The peak, average, and minimum pressures lie on parallel straight-line segments Therefore, on each segment they obey equations of the form

$$p = k_i K_n^{\beta} \tag{2}$$

where the constant β is the same for the three pressures and a particular value of the constant k_i applies to each It follows that the ratio of peak-to-minimum pressure (i e , the compression wave strength) is independent of nozzle throat size at fixed port diameter (i e , fixed f_w) More generally, results at other values of f_w show that the wave strength is essentially independent of the port-to-throat ratio $1/J$ and of K_n This result is surprising, since losses due to nozzle reflection should increase as $1/J$ approaches unity The strength of the reflected wave would, therefore, be expected to vary from motor to motor and with time in any particular firing The invariance of wave strength at the head-end of the motors suggests that a limiting value is reached during upstream propagation

During stable operation, the nonerosive pressure is given by

$$p = (\alpha \rho_p \, c^* K_n)^{1/(1-n)} \tag{3}$$

where ρ_p is the propellant density and c^* the characteristic velocity The constants α and n refer to a fixed value of the web fraction and to a particular segment of the stable log$P$ vs logK_n plot (see Fig 8) Since Eqs (2) and (3) are of the same form, it follows from Fig 10 that the average effect of the compression wave on the combustion-flow process is equivalent to an increase in n and a decrease in α Consequently, the plot of $\bar{P}_u$ intercepts that of the erosive stable pressure P_c at a particular value of K_n, say K_n^*, which in the present instance is about 220 ††

If a motor operating at $K_n < K^*$ is pulsed, the injected compression wave is attenuated in successive cycles, and the average pressure returns to the stable value On the other hand, when $K_n > K_n^*$, the compression wave is amplified and reaches its limiting strength in a few cycles, whereas the chamber pressure jumps from P_c to the corresponding value of $\bar{P}_u$ For example, a motor operating stably at $P = 610$ psia (i e , $K_n \simeq 400$) is capable of unstable operation at $\bar{P}_u \simeq 1300$ psia Since K_n increases with time for tubularly perforated motors, it is possible for them to be inherently stable during the early portion of a firing and capable of instability at a later time when K has become greater than K_n^* Moreover, if the throat size is decreased in successive firings, K_n^* will be reached at correspondingly earlier times This trend is apparent in the firings shown previously in Fig 9

Data similar to those of Fig 10 are available for $f_w =$ 0 1 and 0 5 The $\bar{P}_c$ lines are close to and parallel to that for $f_w = 0\,8$ and are ordered in the same way as the stable erosive curves The corresponding K_n^* values are 185 and 180 Thus, the combined influence of erosion and of the "humping effect" leads to a small variation of K_n^* with web fraction A part of this variation could have been removed by considering intersections with the nonerosive stable pressure line Since most development motors are erosive, however, K_n^* has been determined in every instance from the intersection of $\bar{P}_{cu}$ and P_c This procedure leads naturally to an approximate critical value of the erosive stable pressure P^* above which the motors enter the pseudostable regime

The foregoing results clearly indicate that K_n^* and P^* can be used as stability criteria provided that scaling, a change of grain cross section, or a change in motor length does not affect the correlation of $\bar{P}_{cu}$ with K_n Experiments that clarify these points are discussed in the sections that follow

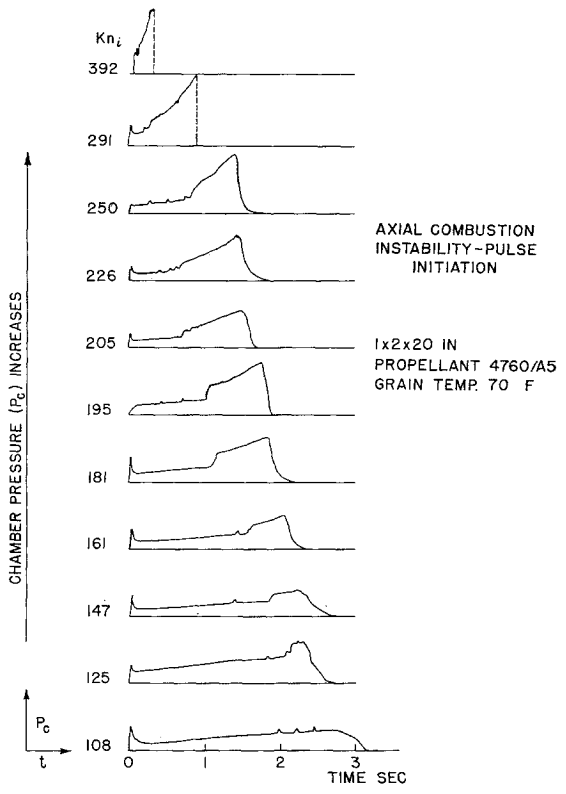

Fig 9 Effect of varying the initial throat diameter

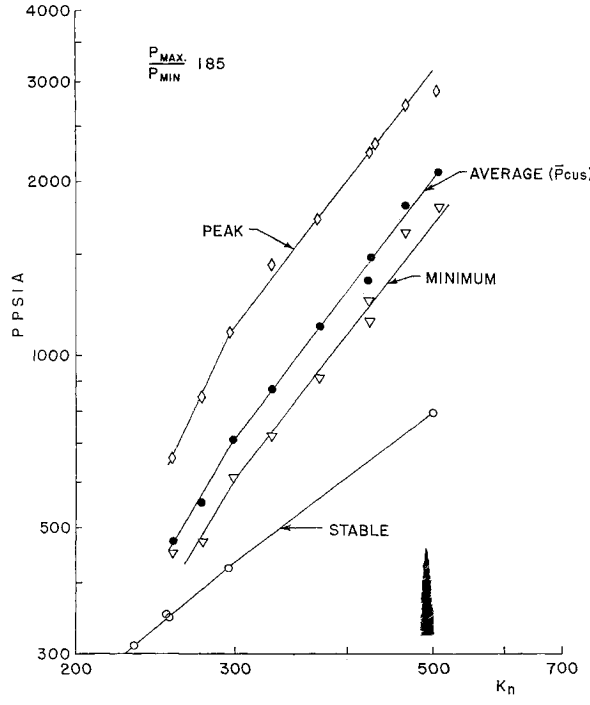

Fig 10 Peak, average, and minimum pressures vs K_n; A_3-× 1-× 2-× 20-in motors at 70°F; $f_w = 0\,8$

†† The computed average values of c^* for stable and unstable operation were in close agreement Since $f_w = 0\,8$ for Fig 10, erosion effects were negligible, and the stable pressure curve agrees with the nonerosive data given in Fig 8

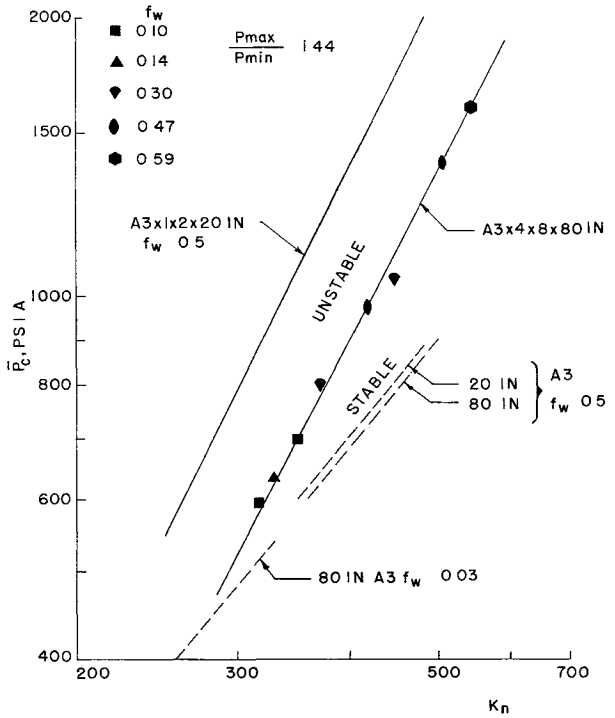

Fig 11 Effect of geometrical scaling

Effect of Geometrical Scaling

In order to determine the effect of scaling by a factor of 4, a series of A_3-× 4-× 8-× 80-in motors was fired for comparison with the A_3-× 1-× 2-× 20-in (f_w = 0 5) motor series The results are given in Fig 11 The data points range from f_w = 0 10 to 0 59 Other data from A_3-× 3-× 8-× 80-in motors covering the f_w range 0 35 to 0 95 are in good agreement with these data; hence the straight line drawn through the data points was not influenced appreciably by the "humping effect" This line lies parallel to, but considerably below, that obtained for the A_3-× 1-× 2-× 20-in motor The shift is associated with a reduction in wave strength, since the ratio of peak-to-minimum pressure decreased from 1 8 (for the smaller motor) to 1 4 As a result, K_n* increased from 180 to 270 and P_c * from 285 to 430 psia It is, therefore, apparent that the larger motor is considerably less prone to instability in the sense that it is inherently stable at a higher operating pressure However, this improvement does not continue proportionally for still larger motors Preliminary data from firings of 17-× 180-in motors indicate that they are, at best, only slightly more stable than the 8-× 80-in size

The influence of the nozzle-end geometry was checked with firings of the A_3-× 3-× 8-× 80-in motor Most 8-in -diam motors were fired using a burst or safety diaphragm adaptor between the casing and the nozzle This introduced an inert channel 5-in -i d × 6-in long between the grain port and the nozzle entrance No change in motor behavior was observed in firings without this device A similar check was made with the 2-× 20-in motor using a scale-size dummy adaptor Motor behavior was unaffected Thus, when fully excited, the motors seem relatively insensitive to discontinuities in the channel area at the nozzle end Similarly, two 1-× 2-× 10-in motors coupled end to end by a short adaptor with a 1-in -diam channel behaved like a single 1-× 2-× 20-in motor except that initiation was more difficult to achiev

Effect of Changi g the Motor Length

For tubularly perforated motors, the ratio of throat-to-port area J is related to the restriction ratio K_n by

$$J = (4/K_n)(L_p/D_p) \quad (4)$$

where L_p is the grain length and D_p the port diameter The port Mach number approaches unity with J, and erosive burning effects increase accordingly Thus, if K_n and D_p are fixed, J increases linearly with L_p, whereas the frequency of oscillation, which varies inversely with L_p, is reduced Nevertheless, it was found that these changes had no effect on the $\bar{P}_{cu}$ vs K_n correlation Firings of B_7-× 3-× 8-× 80- and 120-in motors were made with K_{ni} fixed at 250 Although the stable pressure was considerably higher for the 8-× 120-in motor because of increased erosive burning, $\bar{P}_{cu}$ was in good agreement with data from the 8- × 80-in motor Furthermore, the strength of the compression wave was the same in both motors ‡‡

Similar results were obtained in a comparison of A_3-× 1-× 2-× 20- and 30-in motors $\bar{P}_{cu}$ data at f_w = 0 8 are given in Fig 12 The data are in agreement, indicating that in this instance, also, a 50% increase in length had little effect on unstable operation It was found, however, that a reduction in length to 10 in caused a decrease in wave strength The A_3-× 1-× 2-× 10-in motor firings were not very reproducible (Fig 12), it was difficult to initiate instability, and $\bar{P}_s$ lay well below the 20- and 30-in values In other tests with 2-× 5 5- × 7 5-in motors, instability could not be initiated at K_n values as high as 900 Thus it appears that, although low values of length-diameter ratio tend to inhibit axial instability, at sufficiently high values the influence of grain length is correlated by K_n

Effect of Changing the Grain Cross Section

It has been shown that, for tubularly perforated motors, the time-averaged pressure during axial instability is a function of the restriction ratio In order to verify that this result may be applied more generally, several series of motors were fired with the nontubular grain cross sections shown earlier in Fig 2 For example, data from A_3-× 2-Arm-× 8-× 80-in motors are compared with tubular results in Fig

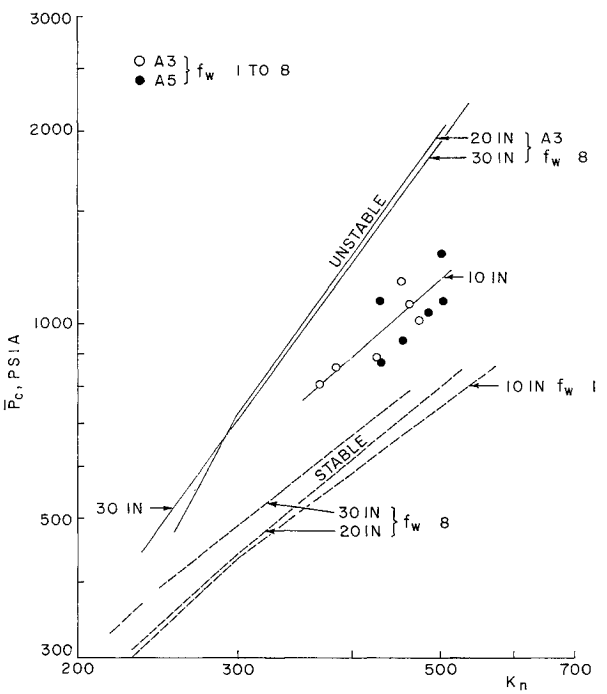

Fig 12 Effect of changing the motor length; A_3-× 1-× 2-× 10-, 20-, and 30-in motors at 70°F

‡‡ The pressure ratios are average values taken at a particular value of f_w They are believed to be accurate to ±5% Ratios falling within this scatter were assumed identical

13 The 2-Arm design is only slightly progressive; hence K_n did not increase much during any given firing, although the internal geometry changed drastically Accordingly, $\bar{P}_{cu}$ remained relatively constant and at the same time agreed with data from the tubularly perforated motors It appears, therefore, that the grain cross section affects the instability primarily through the burning surface area and that this influence is correlated by the restriction ratio

Similar experiments were made using A_3-× slab-× 2-× 20-in motors This design (Fig 2) burns regressively In Fig 14 the unstable portion of each pressure trace is plotted against K_n for comparison with A_3-× 1-× 2-× 20-in results The agreement is generally good, although the instability is somewhat less severe in the slab motor It seems likely that this difference is due to boundary losses at the exposed portions of the casing wall

The foregoing results are supported by other similar data, which, for the sake of brevity, will not be reproduced here It is clear that $\bar{P}_u$ depends strongly on K_n and secondarily, if at all, on such factors as port-to-throat ratio and grain cross section Similarly, the length loses its influence when $L_p/D_p > 10$, whereas scaling effects were observed in the very small motors only Consequently, the parameters K^* and P^* can be used to compare and evaluate the stability characteristics of various propellant formulations as a preliminary step toward prediction in design Furthermore, these data can be obtained most easily from tubularly perforated motors, since a range of K_n values is covered by each firing, and a simple computer program suffices for data reduction The influence of various propellant additives was, therefore, investigated using 4-× 8-× 80-in motors

Influence of Various Propellant Additives

In Fig 15, firing results from 4-× 8-× 80-in motors are plotted for propellants A_3, A_5, A_{12}, C_2, and B_7 The estimated intersections of $\bar{P}_u$ with P are marked with solid circles in each instance The associated K_n^* and P_c^* values are given in Table 2

It is evident that substitution of 5% SAX-3 aluminum alloy for the equivalent amount of oxidizer (propellant A_5) was beneficial in that K_n^* increased from 270 to 430 and P^* from 430 to 760 psia Therefore, although an A_3 motor operating at, say, P = 700 psia would be inherently unstable, the equivalent A_5 motor at the same chamber pressure would almost certainly be inherently stable Substitution of fine pure aluminum rather than SAX-3 (propellant A_{12}) led to a further gain in the maximum stable operating pressure On the other hand, little difference was observed in the behavior of the 1-× 2-× 20-in motor when propellant A_5 was substituted for A_3 Although the explanation of this result is not immediately apparent, it is clear that the subscale motor is not suitable for the evaluation of relative stability characteristics

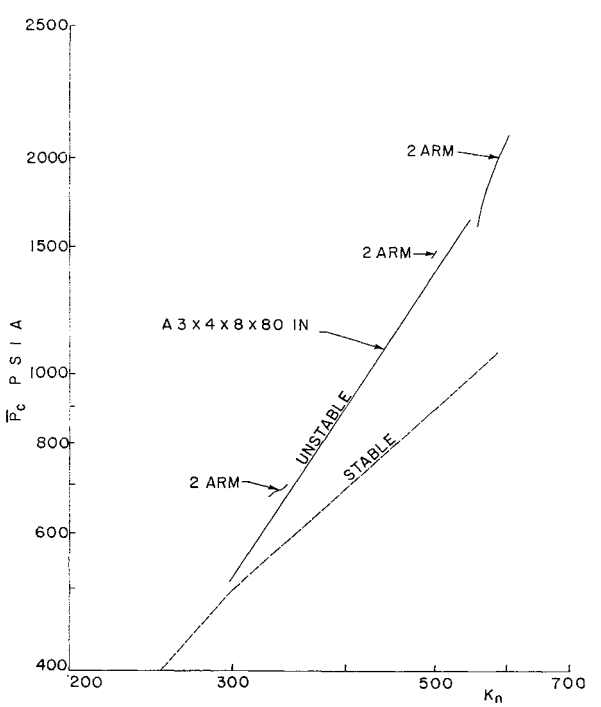

Fig 13 Effect of changing the grain cross section; A_3-× 2-Arm-× 8-× 80-in motors at 70°F

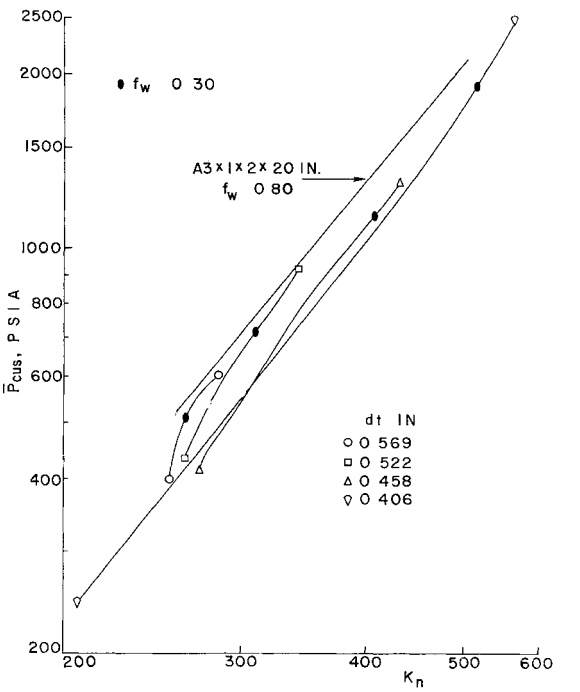

Fig 14 Effect of changing the grain cross section; A_3-× slab-× 2-× 20-in motors at 70 F

The improvement in stability characteristics obtained through the use of aluminum at the 5% level probably does not increase proportionally for higher loadings In fact, there is reason to suspect that too much aluminum is, in a way, as bad as too little Propellant C_2, which contains 19% Al (40 μ, 12% Si), was formulated to give a fairly low burning rate (Table 1) Preliminary data points from 4-× 8-× 80-in and star-× 17-× 180-in firings are given in Fig 15 The data are in fair agreement and indicate that P_c^* is as low as for the nonaluminized propellant, A_3 On the other hand, the instability was not severe, and the gaseous compression wave very weak (pressure ratio of 1 05), so that there was little difference in the slopes of $\bar{P}_u$ and P_{cs} Consequently, the behavior of the motors was relatively insensitive to changes in K_n If the possible influence of the silicon content is discounted, these results suggest that optimum stability characteristics can be obtained at given binder level by adjustment of the aluminum level

At 1000 psia, propellant B_7 burns at approximately the same rate as propellant C_2 The low rate was obtained by the addition of 1 8 parts of LiF to propellant A_5 This modi-

Table 2 K_n^* and P_{cs}^* for various propellants

Propellant	K_n^*	P^*	Additive
A_3	270	430	
A_5	430	760	5% Al (40 μ, 6% Mg)
A_{12}	500	950	5% Al (7 μ)
C_2	approx 310	420	19% Al (40 μ, 12% Si)
B_7	350	390	5% Al (40 μ, 6% Mg) + 1 8 added parts of LiF

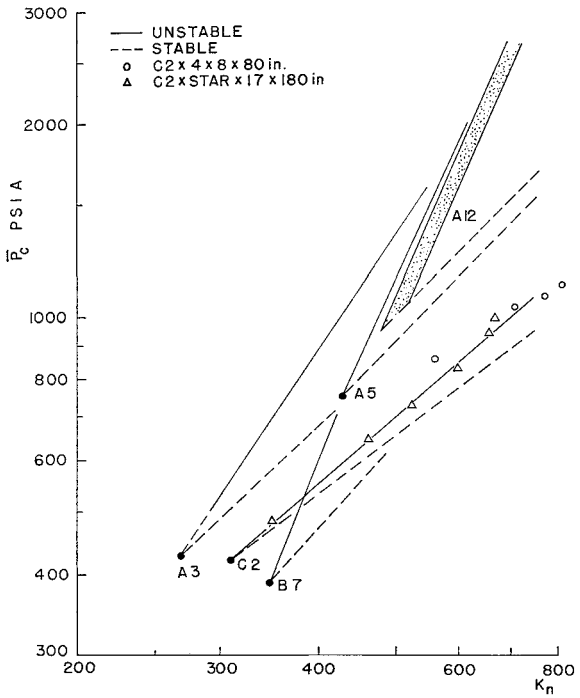

Fig 15 Effect of various additives on stability of the 4-× 8-× 80-in motor; $\bar{P}_{us}$ vs K_n

fication reduced the stable burning rate by about 25% and at the same time produced a drastic deterioration in stability; P_c * decreased from the A_5 value (760 psia) to 390 psia The influence of this change on motor design can be seen by considering Fig 15 Suppose that the burning time of an A_5 motor was to be increased by substituting propellant B_7; assume further that a stable chamber pressure of 700 psia was to be maintained by decreasing the throat area; then the required value of K_n for the B_7 motor would be 540, which corresponds to an unstable chamber pressure of about 1500 psia The design change thus leads to a motor that is inherently unstable to a high degree The ill-fated 17-in firing shown in Fig 4 resulted from such a seemingly innocuous redesign

Examination of Fig 15 and reference to Table 2 shows that the critical pressures for the propellants are ordered in the sequence $B_7 \leftrightarrow C_2$, A_3, A_5, A_{12} It may be seen in Table 1 that the stable burning rates follow the same ordering Thus, it appears that low-burning-rate propellants become unstable at low operating pressures and high-rate propellants at high pressures It seems likely that this behavior can be associated with the erosive burning characteristics of the propellants However, the latter characteristics are not yet available in detail Speculating further, it would not

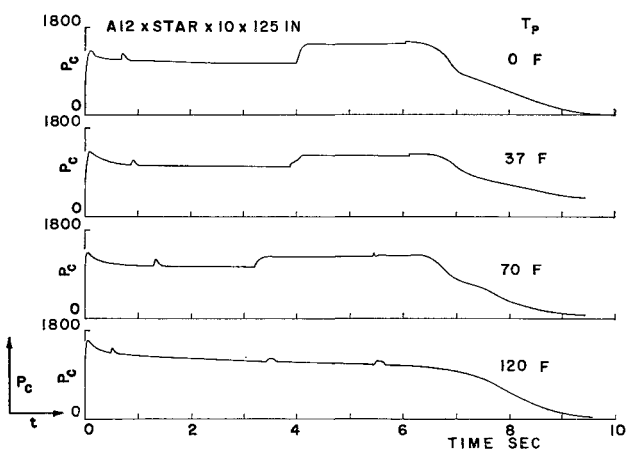

Fig 16 Effect of changing the initial grain temperature

be surprising if the optimum amount of aluminum were that which produces the highest stable burning rate This suggests that burning-rate accelerators should have an important influence on axial instability

Influence of Initial Grain Temperature

All firings discussed so far were made with an initial grain temperature T_p of approximately 70°F As might be expected, the propellant grain temperature affects the stability characteristics of motors In particular, firings of an A_{12}-× star-× 10-× 125-in motor show that with fixed geometry stability decreases with T_p Pressure-time curves for a series of firings with $d_t = 2\ 95$ in are shown in Fig 16 The motor was stable at 120°F and inherently unstable at 70°F and below Evidently, the motor entered the regime of inherent instability at some intermediate temperature Other firings show that with a throat diameter of 3 10 in the critical temperature lies between +10° and −12°F

This behavior does not appear to be due to an increase in $\bar{P}_{cu}$ at given K_n, as may be seen in Fig 17 The data points (shown in relation to A_{12}-× 4-× 8-× 80-in results) were obtained from firings with nozzle throat sizes in the range of 2 95 to 3 10 in All values of K_n were referred to an estimate for the 72°F firing at a time when the fractional pressure integral ϕ reached a value of 0 6 in each instance Hence, the positions of the data points relative to each other are probably correct, although the 72°F base point may be somewhat mislocated No particular trend is evident Certainly the influence of T_p on $\bar{P}_{cus}$ is less than on the stable burning rate This being so, the onset of instability can perhaps be associated with the shift in K_n* arising from temperature displacement of the P_c plot

Further Observations

Several interesting operational features were noted during the course of the experiments, and, although they cannot be reported in detail here, they perhaps merit a brief description

Dual-Wave Systems

Until very recently, all pulse tubes were allowed to fire regardless of when the motor became unstable The precise location of subsequent (secondary) pulses with respect to the traveling wave was of course a matter of chance In general, only a single-wave system persisted in motors using aluminized propellants The secondary pulse merged with the fully developed wave when injected on the rising or decaying part of the waveform Secondary pulses that arrived in the "trough" between reflections produced a new wave that usually decayed but sometimes quickly suppressed the original wave Occasionally both waves were attenuated, and the motor became stable

On the other hand, the A_3-× 4-× 8-× 80-in motor almost always developed a dual-wave system when pulsed secondarily The second compression wave gradually grew stronger while the original wave remained unaffected Eventually, the waves reached equal strength while the wave spacing tended to become symmetrical The presence of two waves caused only a minor increase in $\bar{P}_{cu}$ Similar results were obtained from a firing of an A_3-× 1-× 2-× 30-in motor

Transverse Instability vs Axial Instability

The investigation of transverse (tangential mode) combustion instability reported in Ref 9 showed that the instability became more severe as K_n was increased This trend is the same as for the axial instability discussed here However, the tangential instability did not increase monotonically with K_n as does the axial In fact, a particular value of K_n was found above which the polysulphide motors suddenly became stable No such effect has been observed

in the present investigation However, transverse instability has been observed in a number of firings using the nonaluminized propellant A_3 in the 8-× 80-in motor This has occurred in motors with both 2-Arm and 4-in tubular-grain cross sections These limited results are in agreement with the K_n trend reported in Ref 9

Of perhaps greater interest is the interaction of transverse and axial combustion instability The A_3 firings have demonstrated clearly that transverse instability quickly suppresses axial instability In several firings, transverse instability began when the motors were severely unstable in the axial mode As the transverse oscillations grew, the axial compression waves decayed Furthermore, in two instances the time-averaged pressure increased an additional 50 to 70% over that attained during axial instability

A plausible explanation for this behavior can be made in view of certain experiments reported in Ref 9 and others reported by Price [10] In the first set of experiments, it was found that no burning rate increases were associated with the sloshing-mode oscillations found in opposed-plane-slab motors In this mode of operation, there is no oscillatory component of gas-particle velocity parallel to the surface of the propellant Again, Price found that in a T-burner the maximum increase in burning rate occurred at the gas velocity antinode It is thus reasonable to assume that the burning-rate increases are for the most part due to tangential oscillatory gas flow This being the case, it might be expected that the space-average burning rate would be higher for the tangential mode on the grounds that at any time a greater portion of the burning surface is subjected to high-intensity fluctuations in velocity If this is so and if some limit to the rate increase due to gas velocity is assumed, then the axial shock wave may be unable to sustain itself by virtue of the fact that locally it can produce no rate increase over that arising from the fully developed tangential wave

Summary and Concluding Remarks

The nonlinear nature of finite-wave axial combustion instability can pose a serious threat to development motors Experimental firings of polyurethane-ammonium perchlorate filled motors, in the size range 2-in -i d × 10-in -long to 17-in -i d × 180-in -long, demonstrate that the instability occurs only when initiated by a finite flow disturbance Consequently, normal stable proof firings provide no guarantee that a motor design is inherently stable

During unstable operation, the space-time-averaged burning rate and the means of the fluctuating chamber pressure and thrust are greater than the corresponding quasi-steady values These increases are associated with the presence of a strong gaseous compression wave that propagates longitudinally within the cavity of the motor It appears likely that the increase in burning rate is due largely to the tangential gas velocities induced by the wave

A multiple-pulse technique for the injection of flow disturbances at the head-end of the motors was applied to all firings This apparatus permitted command triggering of instability during pseudostable operation As a result, it was possible to study the phenomenon in a systematic manner

The effect of motor geometry was investigated by changing the motor length, nozzle throat diameter, grain cross section, and scale It was found that the mean value of the fluctuating chamber pressure $\bar{P}_{c\,s}$ was strongly dependent on the restriction ratio K_n The empirical relationship is given by

$$\bar{P}_{cu} = kK_n^{\beta} \qquad (5)$$

where k and β are constants The constants k and β depend primarily on propellant composition and secondarily, if at all, on propellant temperature The intercept of $\bar{P}_{cu}$ and the stable pressure P_c in the $\log P - \log K_n$ plane defines a critical value of the restriction ratio K_n^* and of the stable pressure P_c^* Motors for which $K_n < K_n^*$ and $P < P_c^*$ throughout firing are inherently stable with respect to the nonlinear axial mode

The stability characteristics of motors using propellants for which β is large are extremely sensitive to changes in K_n Thus, a motor with K_n only slightly greater than K_n^* may be unstable to an appreciable degree In such an instance, a minor increase in nozzle throat area will stabilize the design

The use of the experimental stability parameter K_n^* in design prediction hinges on a knowledge of scaling factors The 2-in -diam motor was found to be more unstable than an 8-in motor, whereas limited results from 8-in and 17-in motors were in general agreement At the same time, substitution of 5% of aluminum powder for oxidizer had practically no influence on the instability characteristics of the 2-in motor and yet proved beneficial in the larger motors Consequently, although the 2-in motor is unsuitable for evaluation of stability characteristics, the 8-in firing results can be used for the prediction of stability of motors to at least the 17-in size

Certain results obtained with the 2-in -diam motors indicate that low values of the length-diameter ratio favor stability

The addition of aluminum powder to the propellant did not suppress axial instability All propellants tested, including one with 19% aluminum content, could support instability at sufficiently high restriction ratios The addition of aluminum, however, shifted the critical pressure level above which the motors became inherently unstable The results indicate that the critical pressure level is higher for faster-burning propellants This suggests that the optimum type and level of aluminum alloy may be those which produce the fastest stable burning rate Similarly, the use of burning-rate accelerators may prove beneficial

The stable burning rate of one aluminized propellant was reduced by incorporating 1 8 added parts of lithium fluoride This modification reduced the critical pressure level drastically and led to a propellant that was capable of extremely violent instability at practicable K_n levels

The stability characteristics of one motor design were adversely affected by a reduction in propellant temperature T_p Tests with a star-center 10-in -diam motor indicate

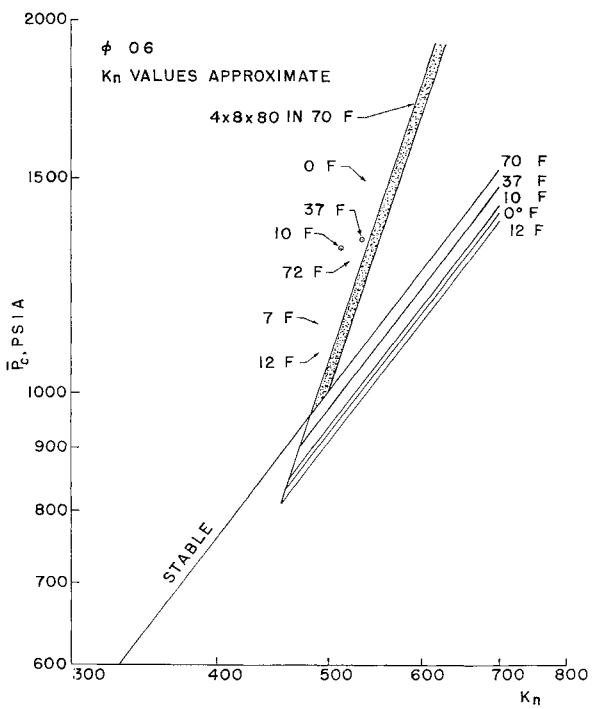

Fig 17 Influence of propellant temperature; A_{12}-× star-× 10-× 125-in motor

that the relation between $\bar{P}_u$ and K is essentially independent of T_p It appears that K_n* shifts to lower values because of the temperature displacement of the stable pressure Thus, although firings at high temperatures were stable, the motor became inherently unstable at a sufficiently low value of T_p

References

[1] Jackson, F and Brownlee, W G., "The 9KS11000 rocket engine for the Black Brant III (U), Interim report—First ten firings, Part II—Ballistic design and combustion instability investigations," Canadian Armament Research and Development Establishment Tech Memo 653/62 (1962); unclassified

[2] Morris, E P, personal communication, Test and Evaluation Section, Propulsion Wing, Canadian Armament Research and Development Establishment (1963)

[3] Dickinson, L A and Jackson, F, "Studies on combustion of polyurethane propellant in rocket motors," 9th Tripartite AXP Res Conf, Vol IV (April 1959); confidential

[4] Dickinson, L A, "Command initiation of finite wave axial combustion instability in solid propellant rocket motors," ARS J **32**, 643–644 (1962)

[5] Dickinson, L A, Brownlee, W G, and Jackson, F, "CARDE investigations of finite wave axial combustion instability," Canadian Armament Research and Development Establishment TN 1459/62 (1962); unclassified

[6] Brownlee, W G, "An experimental investigation of finite wave axial combustion instability (U)" Canadian Armament Research and Development Establishment Tech Memo 660/63 (1963); unclassified

[7] Morris, E P, "A pulse technique for evaluation of combustion instability in solid propellant rocket engines, unclassified paper in course of publication by Canadian Armament Research and Development Establishment

[8] Jackson, F, personal communication, Rocket Engine Development Section, Propulsion Wing, Canadian Armament Research and Development Establishment (1963)

[9] Brownlee, W G and Marble, F E, "An experimental investigation of unstable combustion in solid propellant rocket motors," *ARS Progress in Astronautics and Rocketry: Solid Propellant Rocket Research*, edited by M Summerfield (Academic Press Inc, New York, 1960), Vol 1, pp 455–494

[10] Price, E W, "Combustion instability in solid propellant rocket motors," Naval Ordnance Test Station NAVORD Rept 7023 (NOTS TP 2389) (1959); unclassified

FEBRUARY 1964 AIAA JOURNAL VOL 2, NO 2

Comparison of Commercial, Spherical Powder, and Wire Bundle Tungsten Ionizers

GUNTIS KUSKEVICS* AND BARRY L THOMPSON†
Electro Optical Systems, Inc Pasadena, Calif

Cesium ionization on different porous tungsten structures was measured in terms of neutral fraction, critical temperature, and flow rate in the 10^{-6}-torr range These structures included $\frac{3}{16}$-in commercial sintered ionizers with about 2-μ average pore diameter, spherical powder ionizers of 6-μ effective pore diameter, and 12- and 6-μ-diam wire bundle ionizers Conductance was measured at room temperature with nitrogen and at operating temperature with cesium vapor Ion current and neutral fraction were plotted as log$j$ or logα vs $1/T$, which allows easier extrapolation of the critical temperatures The directly heated ionizers could be operated up to 1500°C In general, the performance of ionizers improved with time of operation During this conditioning time, the critical temperature and neutral fraction decreased The best critical temperatures for all tungsten ionizers in the 10^{-6}-torr residual gas pressure at current densities between 1 and 30 ma/cm^2 were within 100°K of Langmuir's data for solid tungsten The critical temperature had a considerable spread Neutral fractions for commercial sintered, spherical powder, and fine wire bundle ionizers ranged from 0 1 to 15% but were considerably higher for coarse wire bundle ionizers The angular distribution measurements of neutral fraction were used to select the best angular position of a neutral efflux detector for neutral fraction measurements and to test the validity of the assumption that the relative angular distribution remains independent of whether a beam is being extracted

1 Review of Surface Ionization on Porous Tungsten

THE first practical cesium ionizers in the early ion sources, surface ionization detectors, and even ion propulsion devices used solid tungsten filaments or ribbons Surface ionization of the alkali metals on solid refractory metal surfaces has been reviewed recently by Zandberg and Ionov [1] A brief review of surface ionization on other solid materials was given previously [2]

Studies of porous ionizers started with the application of commercial porous tungsten in ion engines in late 1958 At the same time, theoretical studies of surface ionization on idealized porous structures determined that the desirable pore size should be less than 1 μ [3–5]

More basic experiments with porous ionizers were performed later The first of these, by Stavisskii and Lebedev,[6] used a relatively large (10-mm diam, 2-mm thick) porous tungsten disk of 70% of theoretical density, made of a very fine 1-μ grain size

The ion current-ionizer temperature curves were similar to those for solid tungsten Following the definitions of dif-

Presented as Preprint 63016 at the AIAA Electric Propulsion Conference, Colorado Springs, Colo, March 11–13, 1963; revision received October 7, 1963 This work has been supported by NASA Contracts NAS8 2547 and NAS8-1537 and Air Force Contract AF 33(616)-6958 Spherical powder and wire bundle ionizers were developed by H Todd and M LaChance

* Senior Scientist Associate Fellow Member AIAA
† Physicist